PAPER

Check for updates

Uniquely sized nanogels *via* crosslinking polymerization†

Disraëli N. M. Kusmus, [ID] [a] Thijs W. van Veldhuisen, [ID] [a] Anzar Khan, [ID] [b] Jeroen J. L. M. Cornelissen [ID] *[a] and Jos M. J. Paulusse [ID] *[a]

Nanogels are very promising carriers for nanomedicine, as they can be prepared in the favorable nanometer size regime, can be functionalized with targeting agents and are responsive to stimuli, *i.e.* temperature and pH. This induces shrinking or swelling, resulting in controlled release of a therapeutic cargo. Our interest lies in the controlled synthesis of functional nanogels, such as those containing epoxide moieties, that can be subsequently functionalized. Co-polymerization of glycidyl methacrylate and a bifunctional methacrylate crosslinker under dilute conditions gives rise to well-defined epoxide-functional nanogels, of which the sizes are controlled by the degree of polymerization. Nanogels with well-defined sizes (polydispersity of 0.2) ranging from 38 nm to 95 nm were prepared by means of controlled radical polymerization. The nanogels were characterized in detail by FT-IR, DLS, size exclusion chromatography, NMR spectroscopy, AFM and TEM. Nucleophilic attack with functional thiols or amines on the least hindered carbon of the epoxide provides water-soluble nanogels, without altering the backbone structure, while reaction with sodium azide provides handles for further functionalization *via* click chemistry.

1. Introduction

The emergence of nanomedicine brought about personalized medicine by combining nanotechnology and medicine.[1,2] The field of theranostics applies nano-sized macromolecules to combine controlled administration of therapeutic drugs with diagnostics.[3] Polymer nanoparticles are particularly interesting to this end as their physical properties, structure and composition can be controlled.[4] These nanoparticles are readily rendered hydrophilic and biocompatible, and can be designed to encapsulate and release therapeutics.[5] Polymer nanoparticles such as nano-sized hydrogels, also coined nanogels – are crosslinked, spherical, three-dimensional soft materials that are highly modular in nature. Nanogels displaying high water content, large surface area, high loading capacity, internal network, good stability in biological fluids and responsiveness to external stimuli.[6–8] Desirable properties such as biodegradability, blood compatibility and amphiphilicity can be built in.[9,10] The size, surface charge, porosity, softness and density can be tuned. As such nanogels have found use in tissue engineering,[7,11,12] vaccines, cancer treatment,[13–16] bioimaging,[17,18] antifouling,[19,20] ophthalmic diseases,[21] biosensing,[18,22–28] pain management,[29] and nucleic acid delivery systems.

There are several ways to synthesize nanogels, such as emulsion polymerization, precipitation polymerization,[30,31] inverse nanoprecipitation,[32,33] self-assembly[9] and template assisted polymerization.[34] To achieve optimal cellular uptake and biodistribution, nanoparticles should be between 10 – 100 nm in diameter.[35,36] Others have succeeded in forming nanogels of well-defined uniform size.[37] However their strategies either require multiple steps to form nanogels,[38–40] surfactants[41,42] or produce a single size per reaction performed.[43] Controlled crosslinking polymerization methods with multifunctional monomers provide excellent control over the resulting nanogels, as reaction conditions such as reaction time and monomer concentration determine the size of the nanogel.[44] Controlled radical polymerization techniques, such as ATRP and RAFT slow the reaction rate to promote the formation of uniform particles.[45,46] These strategies, that provide easy access to well-defined polymeric nanoparticles with uniform composition over the entire 10–200 nm size regime, have been reported for core–shell nanogels and hyperbranched polymers[47,48] but not for nanogels. Good control over nanogel size is highly desirable in biomedical applications as it determines ease of endosomal escape.[49–51]

Cellular uptake and biodistribution behavior of nanogels is strongly affected by the type of surface functionality.[5] Factors such as polarity and surface charge determine the hydrophilicity of the nanogel as well as its circulation in blood.[52] Other structural properties such as useful functional groups aid the

[a]MESA+ Institute for Nanotechnology and TechMed Institute for Health and Biomedical Technologies, Department of Biomolecular Nanotechnology, University of Twente, Drienerlolaan 5, 7522, Enschede, NB, Netherlands. E-mail: j.j.l.m. cornelissen@utwente.nl; j.m.j.paulusse@utwente.nl

[b]Korea University, 145 Anam-ro, Anam-dong, Seoul, Seongbuk-gu, Korea

attachment of targeting molecules and contrast agents.[53] Synthesizing nanogels with built in handles provides a versatile template able to be modified to functional nanogels, such as vaccine transport vehicles.[6,54] Epoxides are highly reactive groups resulting from the three-membered ring with high ring strain.[55] As such epoxides readily undergo ring–opening reactions with a wide array of nucleophiles.[56]

In this work, we describe the development of uniquely sized epoxide-functional precursor nanogels *via* controlled cross-linking polymerization. In a subsequent post-formation step, the epoxide moieties are functionalized with various amines, azides and thiols, as well as hydrolyzed to the corresponding diol. This provides a platform for the formation of versatile functional nanogels as carriers.

2. Results and discussion

2.1 Synthesis of GMA-EGDMA nanogels

GMA-EGDMA nanogels (NGs) were prepared by RAFT copolymerization of glycidyl methacrylate (GMA) and ethylene glycol dimethacrylate (EGDMA) in a 3 : 1 mole ratio under dilute conditions (5 wt%)(Scheme 1).

Monomer conversion was determined by ^{1}H NMR spectroscopy, by integrating the characteristic signals of the alkene groups located at $\delta = 6.1$ and 5.7 ppm. NG size was determined by dynamic light scattering (DLS). Fig. 1 shows the NG diameter as a function of conversion, revealing gradual NG growth. All NGs had a PDI of 0.2. Branching and pre-NG clusters are formed starting from 0% conversion up to 20% (for this particular system). Afterwards well-defined NGs are formed that continue growing while maintaining narrow dispersity.[57] Eventually stagnation in particle size occurs at higher monomer conversions, followed by the formation of a macrogel. Four representative samples were prepared and studied with 21, 26, 42 and 47% conversion, respectively, labeled **GMA-EGDMA-21** and so on. Size exclusion chromatography (SEC) analysis on **GMA-EGDMA** NGs revealed broad size distributions that shift to shorter elution times with increasing monomer conversion. Due to the branches and crosslinks in the prepared NGs, the elution times cannot be related to linear polymer standards. Moreover, although the exclusion limit of the employed SEC column is over 4×10^7 g mol^{-1}, the shape of the distribution indicates that the NGs surpass the exclusion limits.

The morphologies of **GMA-EGDMA** NGs were further analyzed by microscopy techniques. The TEM and AFM images of **GMA-EGDMA-47** is highlighted below in Fig. 2 analysis of the TEM image gave a mean diameter of 17 nm. AFM indicated
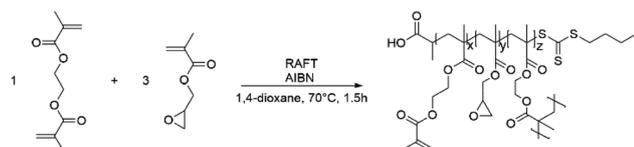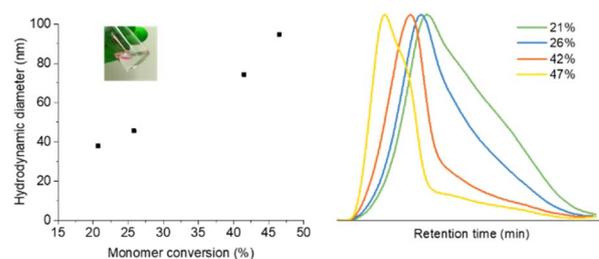

Fig. 1 Hydrodynamic diameter of **GMA-EGDMA** NGs as a function of monomer conversion. Inset: **GMA-EGDMA** in 1,4-dioxane solution (left). Size exclusion chromatography traces of **GMA-EGDMA** NGs at increasing monomer conversion (right).

a mean diameter of 20 nm and a mean particle height of 3 nm. These results combined the with DLS data in Fig. 1 demonstrate the malleability and responsiveness of the synthesized NGs. These NGs swell in solution becoming spherical in shape (DLS). Once casted onto a surface and dried, the NGs flatten out and take up a disc-like shape.[58] This phenomenon is observed both at ambient pressure (AFM) as well as under vacuum (TEM).

^{1}H NMR spectroscopy on **GMA-EGDMA** NG, reveals characteristic signals corresponding to the epoxide moieties, from which a concentration of residual methacrylates of 1.10 mmol g^{-1} is calculated. Comparison of the signals at $\delta = 4.3$ ppm (4H from EGDMA and ^{1}H from GMA) to those at $\delta = 3.8$ ppm (^{1}H from GMA), gives an EGDMA:GMA incorporation ratio of approximately 1 : 3, which is in accordance with the feed ratio(Fig. 3).

NG formation also proceeds as described above in the presence of a third monomer. In the case of a monomer with a methacrylate functionality such as DMAEMA, it will be covalently incorporated into the NG structure. As known from the literature, NGs and other nanoparticles often encounter stability issues, resulting in aggregation.[59] Particles with reactive groups tend to crosslink, while dried solid particles may no longer be redispersed. To assess the stability of the NGs formed, DLS measurements were repeated over time. The dried NGs were readily dissolved in various organic solvents (DMF, DMSO, 1,4-dioxane, CHCl$_3$, DCM, acetone) and DLS analysis did not show signs of degradation or decomposition (no changes in
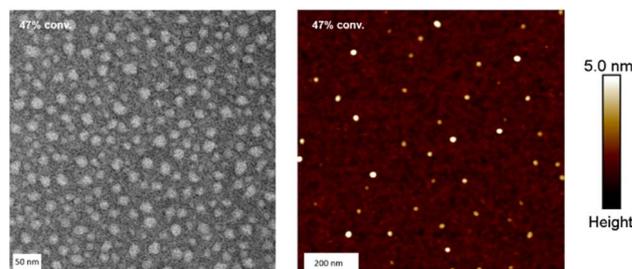

Fig. 2 TEM image of **GMA-EGDMA** NG (on the left) displaying round particles with a mean diameter of 17 nm. AFM image (on the right) likewise indicates the formation of round, disc-like particles with a mean diameter of 20 nm and a mean height of 4 nm. The scale bars are 50 nm and 200 nm for TEM and AFM, respectively.
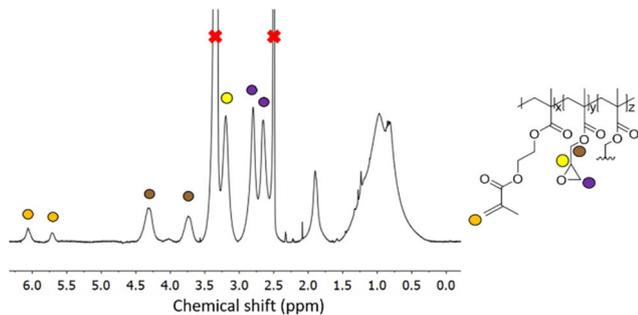

Scheme 1 The RAFT polymerization of EGDMA with GMA forming **GMA-EGDMA** nanogels.

Fig. 3 ^{1}H NMR spectroscopy of a representative **GMA–EGDMA** sample at 29% monomer conversion, with characteristic epoxide signals at $\delta = 3.2$ ppm, 2.8 ppm and 2.7 ppm in DMSO-d$_6$.

hydrodynamic diameter or PDI) even after storing for 6 months at room temperature in dried state.

2.2 Functionalization of GMA-EGDMA nanogels

Having demonstrated the controllability and robustness of this system we proceeded to functionalization of the epoxide moiety by exploiting its reactivity and ring strain to demonstrate the versatility of these NGs.[60] All functionalizations and reactions mentioned hereafter were done on **GMA-EGDMA** NG of which the remaining methacrylates were quenched with excess AIBN. The hydrodynamic particle diameter of these NGs was 41 nm as determined by DLS in 1,4-dioxane(Scheme 2).

The epoxide moieties on the NGs were hydrolyzed in order to render the NGs water-soluble. Reaction with excess TFA and water at room temperature resulted in **GMA-EGDMA-OH** NG. ^{1}H NMR spectroscopy no longer displayed the characteristic epoxide signals, indicating complete conversion, while new signals at $\delta = 4.7$ and $\delta = 4.9$ ppm are in agreement with alcohol groups on the hydrolyzed epoxide. However, the solubility of **GMA-EGDMA-OH** NG in water remained limited. Foaming is observed, indicating solvation in water. However, even at concentrations as low as 0.12 mg mL^{-1} some sedimentation was observed. We suspect that there are two reasons for this phenomenon. Weaver and coworkers demonstrated that degree of polymerization (DP) plays a significant role in water-solubility
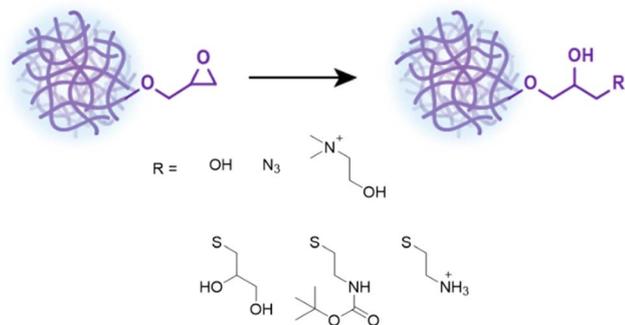
of HEMA homopolymers bearing pendant hydroxyl groups like **GMA-EGDMA-OH**.[61] The DP of the sedimented **GMA-EGDMA-OH** particles was likely too high rendering these NGs insoluble in water. Likewise, the ratio between the hydrophilic hydroxyl groups and the hydrophobic crosslinker and backbone of the sedimented NGs is too low to properly solvate these NGs. The variations in solubility indicate the formation of slightly different NG particles. Those NGs containing a higher ratio of epoxide moieties and thus more hydroxyl groups after hydrolysis are water-soluble, whereas those with fewer epoxide groups remain insoluble in water after hydrolysis. Likewise, **GMA-EGDMA-OH** NGs with a lower DP are water-soluble. DLS measurements in DMF gave a particle diameter of 104 nm. Such a significant increase in size is expected for a more polar NG in a polar solvent with intrinsic swelling abilities. The increase in PDI further suggests the formation of slightly different particles. Various amounts of epoxide moieties and thus hydroxide groups after hydrolysis, mean varying amounts of swelling, resulting in a variety of **GMA-EGDMA-OH** particle sizes and thus an increase in PDI(Fig. 4).

Khan and coworkers have extensively researched the opening of epoxides with thiols, utilizing LiOH as a catalyst.[62–66] To further probe the water-solubility of these NGs, the choice was made for 1-thioglycerol as the thiol reagent, forming **GMA-EGDMA-THG** NG. Stoichiometric amounts of LiOH were needed to achieve full conversion. ^{1}H NMR spectroscopy indicates complete conversion and a successful reaction. DLS measurements in DMSO gave a Z-average of 67 nm. Despite full conjugation of 1-thioglycerol onto the epoxide moieties, the resulting NG did not become appreciably water-soluble. We suspect that the ratio between the alcohol groups and the hydrophobic EGDMA crosslinker and methacrylate-based polymer backbone is too low to achieve (complete) water-solubility.

Alternatively, water-solubility can be achieved by introducing charge. **GMA-EGDMA-Boc** NG was synthesized as 2-(Boc-amino)ethanethiol has a recognizable signal on ^{1}H NMR spectroscopy as well as the added benefit of becoming water-soluble upon deprotection. ^{1}H NMR spectroscopy of **GMA-EGDMA-Boc** NG indicates complete conversion. DLS measurements in DCM gave a Z-average of 75 nm. The increase in NG size is likely due

Scheme 2 Functionalization of **GMA-EGDMA** NG through acid catalyzed epoxide ring opening, ring opening with sodium azide or tertiary amines, and ring opening with functional thiols.
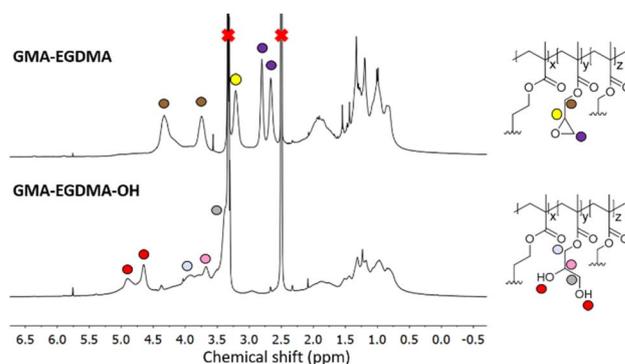

Fig. 4 ^{1}H NMR spectroscopy of **GMA-EGDMA-OH** NG (bottom) indicating full conversion as well as the presence of hydroxyl groups at $\delta = 4.9$ ppm and $\delta = 4.7$ ppm.
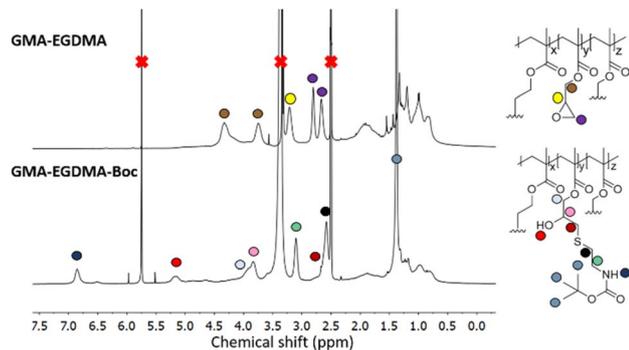
Fig. 5 ^{1}H NMR spectra of NGs before (**GMA-EGDMA**) and after conjugation of 2-(Boc-amino)ethanethiol (**GMA-EGDMA-Boc**).

to the bulky Boc group. Boc-deprotection was achieved with excess TFA resulting in **GMA-EGDMA-NH$_3$$^+$** NG, as confirmed by the disappearance of the ^{1}H NMR signal at $\delta = 1.4$ ppm corresponding to the 9 protons from the Boc group (data not shown). This cationic NG is fully water-soluble, with a hydrodynamic particle diameter of 91 nm in H$_2$O and a high surface charge of +37 mV in 10 mM HEPES solution(Fig. 5).

Amines are also capable of nucleophilic attack on an epoxide and have been successfully used in post-polymerization functionalization. Xu and coworkers functionalized pGMA with various amines to synthesize nonviral transfection vectors for gene therapy.[67–71] Literature indicates however that crosslinking occurs most likely due to further functionalization of the amine.[72–74] As such a tertiary amine was chosen for the formation of **GMA-EGDMA-NR$_3$$^+$** NG. ^{1}H NMR spectroscopy exhibits no epoxide signals, indicating complete conversion, as seen in Fig. 6. A signal at $\delta = 3.3$ ppm corresponds to the methyl groups on the quaternized amine. This cationic NG is water-soluble and displays a highly positive surface charge of +30 mV in 10 mM HEPES. DLS measurements in H$_2$O gave a Z-average of 170 nm indicating characteristic swelling in water.[75]

Tsarevsky and coworkers provide a protocol for the functionalization of the glycidyl methacrylate epoxide with sodium azide.[76] Azides are a popular functional group as they can undergo azide–alkyne click reactions with various alkynes, installing radioactive tracers, targeting ligands and more.
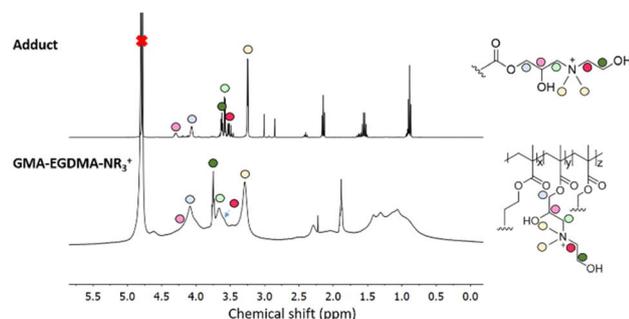

Fig. 6 ^{1}H NMR spectrum of **GMA-EGDMA-NR$_3$$^+$** in comparison with the ^{1}H NMR spectrum of its N,N-dimethylethanolamine adduct indicates a successful reaction and complete conversion.

Ammonium chloride is utilized to protonate the alkoxide anion, preventing any possible crosslinking.[77] The ^{1}H NMR spectrum of **GMA-EGDMA-N$_3$** NG displays no epoxide signals at $\delta = 3.2$ ppm, 2.8 ppm and 2.7 ppm – indicating complete conversion. The signals for the methylene adjacent to the azide group (–CH$_2$N$_3$) can be observed at $\delta = 3.3$ ppm. ^{1}H NMR spectroscopy was also conducted in DMF-d$_7$. The resulting spectra are comparable to those found in literature.[76] The ^{13}C NMR spectroscopy signal indicative of a carbon next to the azide moiety (CH$_2$N$_3$) can be observed at $\delta = 53$ ppm in DMSO-d$_6$ and at $\delta = 55$ ppm in DMF-d$_7$ (Fig. S1 and S2† respectively in ESI†). In addition, a distinctive azide signal is observed by FT-IR at 2104 cm^{-1}. A broad peak at 3400 cm^{-1} corresponding to the hydroxyl group further confirms successful epoxide opening(Fig. 7).

Partial epoxide opening was also carried out with 0.5 equivalents of sodium azide to assess quantitative reactivity and control over functionalization. The FT-IR spectrum in Fig. 8 (middle) displays an azide peak at 2104 cm^{-1}, an OH peak at
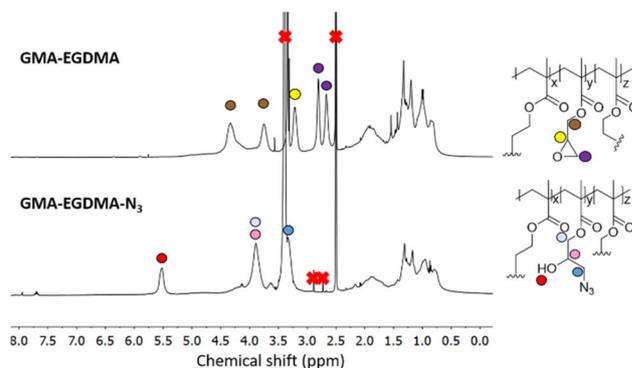
Fig. 7 The ^{1}H NMR spectrum of **GMA-EGDMA**-N$_3$ (bottom) in DMSO-d$_6$ indicates no more epoxides present and thus full conversion.
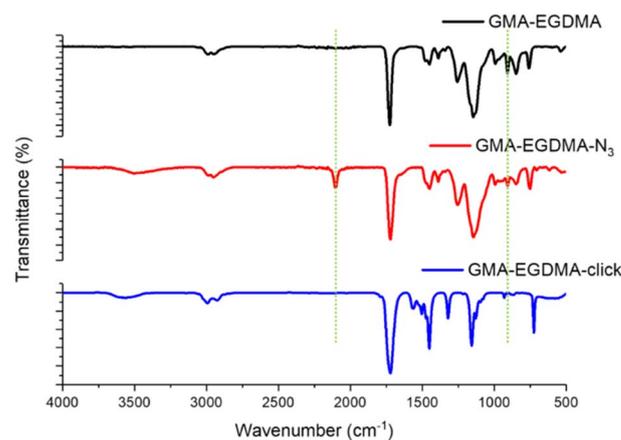
Fig. 8 The. The top IR spectrum displays the **GMA-EGDMA** NG prior to undergoing post-synthesis modifications, displaying an epoxide peak at 907 cm^{-1}. In the middle spectrum the emergence of a hydroxyl group can be seen at 3400 cm^{-1} as well as an azide group at 2102 cm^{-1} after reacting with sodium azide. A subsequent click reaction of the azide moieties results in the disappearance of peak at 2102 cm^{-1} as can be seen in the bottom spectrum.
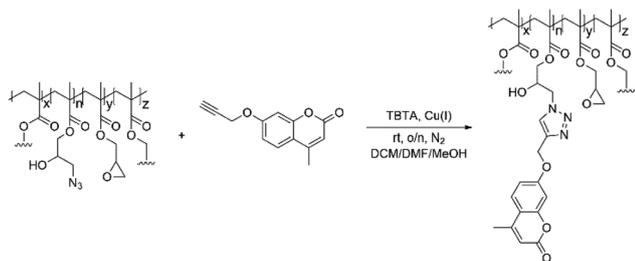
Scheme 3 GMA-EGDMA-N$_3$ NGs with residual epoxide groups were clicked with alkyne-coumarin under inert conditions. Tetrakis(aceto-nitrile)copper(ı) hexafluorophosphate and TBTA catalyzed the reaction.
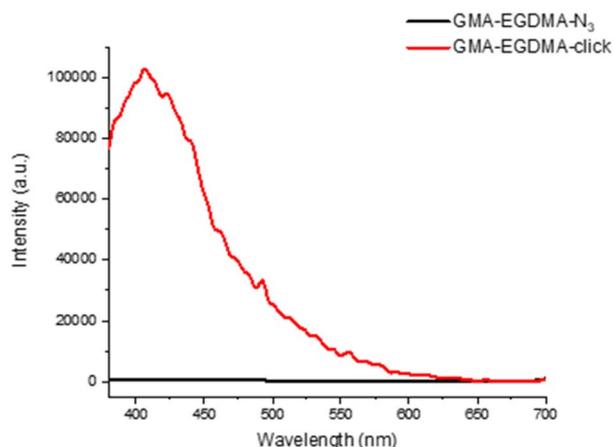
Fig. 9 Comparing the fluorescence spectra of GMA-EGDMA-N$_3$ before and after the reaction with a pro-fluorescent coumarin dye indicates a significant increase in fluorescence intensity. Both NGs were measured at 3 mg mL^{-1} in DMF, exciting at $\lambda = 360$ nm and detecting the emission at $\lambda = 380$ nm–700 nm.

3370 cm^{-1} and C=O peak at 1721 cm^{-1}. The residual epoxide peak at 907 cm^{-1} is also present. ^{1}H NMR spectroscopy in DMSO-d$_6$ indicated approximately 43% conversion which is lower than the targeted 50% conversion. This is likely due to a stoichiometric excess needed to drive the reaction forward as well as the error margin of calculations done on NMR spectra of nanoparticles.

In a subsequent reaction the azide groups were clicked with a pro-fluorescent coumarin dye containing an alkyne moiety to assess their accessibility and reactivity when forming part of a complex NG network(Scheme 3).

The FT-IR measurements depicted in Fig. 8 indicate the disappearance of the azide peak at 2102 cm^{-1} (bottom spectrum). It is suspected that the triazole peak is located at 1650 cm^{-1} but is shielded by the large carbonyl peak.[78] The spectra in Fig. 9 display the significant increase in fluorescence of the NG after attachment of the fluorescent molecule.

3.   Conclusions

Herein we describe a novel method for the preparation of epoxide containing NGs that are robust and size-controllable.

GMA-EGDMA NGs can be synthesized with a particle diameter between 38 and 95 nm. The polydispersity witnessed on TEM and GPC suggests that this method is quite sensitive and requires fine-tuning. Computational models and kinetics experiments should further elucidate intricacies influencing steady NG growth and reproducibility. Nevertheless, NGs formed *via* this method are highly robust and stable. They can withstand freeze-drying and solvent removal *in vacuo* and once redissolved months later, retain their original size. The epoxide moiety incorporated in the NG remains accessible and can undergo post-polymerization modifications with amines, thiols, TFA and azides to a wide variety of versatile functional NGs. An increase in PDI of the resulting NGs suggests that some reactions are better tolerated than others. Water-soluble NGs are easily achieved by introducing permanent charge. The formation of charged NGs allows modification of its surface polarity and thus its efficacy in blood. This work serves to further illustrate the versatility achievable with polymeric NGs combined with increased efficiency and control when synthesized in a single step *via* a living polymerization with monovalent and divalent vinyl monomers.

4.   Experimental

4.1   Materials and methods

Glycidyl methacrylate (GMA, 97%) and ethylene glycol dime-thacrylate (EGDMA, 98%) were purchased from Sigma-Aldrich and passed through a column of neutral Al$_2$O$_3$ prior to use. *N,N*-dimethylformamide (DMF, anhydrous, 99.8%), trifluoro-acetic acid (TFA, HPLC grade, >99.0%), *N,N*-dimethylethanol-amine (redistilled, 99.5%), 1,4-dioxane (HPLC grade, >99.5%), azobisisobutyronitrile (AIBN, 98%), 2-(Boc-amino)ethanethiol (97%), lithium hydroxide (LiOH, reagent grade, 98%), tris((1-benzyl-4-triazolyl)methyl)amine (TBTA, 97%) and tetrakis(ace-tonitrile)copper(ı) hexafluorophosphate (Cu(CH$_3$CN)$_4$PF$_6$, 97%) were purchased from Sigma-Aldrich and used without further purification. Sodium azide (NaN$_3$, 99%) was purchased from Acros Organics and used as supplied.‡ 4-methyl-7-(prop-2-yn-1-yloxy)-2H-chromen-2-one was purchased from MolPort as used without any further purifications. Dichloromethane (DCM, 99.7%) and methanol (MeOH) were obtained from Ossum Chemicals. Demi-water was used unless stated otherwise. The RAFT agent 2-[[(butylthio)thioxomethyl] thio] propanoic acid was synthesized following a literature procedure.[79]

4.2   Nuclear magnetic resonance

Monomer conversions were determined by ^{1}H NMR spectros-copy in DMSO-d$_6$ or CDCl$_3$ on a Bruker Avance 400 MHz spec-trometer. The signals of the deuterated solvents were used as a reference. Monomer conversions were calculated either by preparing an ^{1}H NMR sample with 20 mg NG, CDCl$_3$, along with

---

‡ Safety note: Large scale reactions of azide are prone to dangerous exothermic reactions. The use of chlorinated solvents in the presence of sodium azide must be avoided, as the byproducts may be highly explosive.[81]

25 μL of DMF as internal standard or by collecting the unreacted monomers during precipitation.

4.3 Dynamic light scattering

Hydrodynamic diameters were measured by dynamic light scattering (DLS) using a Malvern Instruments Zetasizer ZS at a backscatter angle of 173° and taking the Z-average in intensity. Measurements were done in triplicate, employing PEG/PiBMA as control. Zeta potential was measured on the same equipment at 20 °C in water employing folded capillary cells.

4.4 Fourier transform infrared spectroscopy

Infrared spectroscopy (FT-IR) was performed on a Bruker Alpha and analyzed with OPUS software.

4.5 Transition electron microscopy. Transition electron microscopy (TEM) samples were prepared with a concentration of 0.8 mg mL^{-1} in 1,4-dioxane, of which 5 μL was casted on a copper grid. The sample was subsequently stained with a 1 w/v% MilliQ solution of uranyl acetate for 35 seconds. Excess staining was removed with a filter paper. TEM images were collected on a Philips CM300ST-FEG transmission electron microscope 300 kV equipped with GATAN Ultrascan1000 (2kx2k CCD camera) and GATAN Tridiem energy filter (2 K × 2 K CCD camera). The TEM images were analyzed with ImageJ software by measuring the diameters of 200 individual NG spheres and calculating the average size and standard deviation. Dialysis was done using Spectra/Por 6 Dialysis Membrane Pre-wetted RC Tubing with a molecular weight cut-off of 1 kDa.

4.6 Size exclusion chromatography

Size exclusion chromatography (SEC) was performed on a Waters e2695 Separations Module equipped with an Agilent PLgel 20 μm MIXED-A 300 × 7.5 mm column, a Waters photodiode array detector (PDA 2998), a fluorescence detector (FLR 2475) and a refractive index detector (RI 2414). Samples were dissolved in HPLC grade chloroform (eluent) to a concentration of 2.0 mg mL^{-1} and filtered with a GE Healthcare Whatman SPARTAN 13/0.2 RC 0.2 μm syringe filter. An injection volume of 100 μL was applied along with an elution speed of 1 mL min^{-1} at 35 °C. Molecular weights and PDI were calculated from linear polystyrene calibration standards.

4.7 Synthetic procedures

4.7.1 GMA-EGDMA NG formation. RAFT agent 2-[[(butylthio)thioxomethyl] thio] propanoic acid (248.8 mg, 1 mmol, 1 equiv.), AIBN (34.3 mg, 0.2 mmol, 0.2 equiv.), GMA (5.2 mL, 39.2 mmol, 37.5 equiv.), EGDMA (2.46 mL, 13.1 mmol, 12.5 equiv.) and 1,4-dioxane (150 mL, 95 w/w%) were added to a 500 mL round bottom flask equipped with a stir bar, sealed with a septum and purged with nitrogen for 45 min. The flask was subsequently placed in an oil bath at 70 °C and allowed to react for 1.5 h after which it was taken out of the oil bath and quenched with 3 mL DCM or excess AIBN (4.42 g, 26.9 mmol) in 1,4-dioxane (30 mL). The NG was precipitated three times in hexane yielding a white solid (unquenched NG 2.06 g, 29%

conversion, 5.51 mmol g^{-1} epoxides, 1.102 mmol g^{-1} dangling methacrylates; quenched NG 2.78 g, 54% conversion, 3.04 mmol g^{-1} epoxides).

4.7.2 GMA-EGDMA-N$_3$ NG formation. GMA-EGDMA NG (101 mg, 0.3 mmol epoxides), sodium azide (40.4 mg, 0.6 mmol, 2 equiv.), ammonium chloride (49.2 mg, 0.9 mmol, 3 equiv.) and DMF (10 mL) were combined in a 25 mL round bottom flask, equipped with a magnetic stir bar, and heated at 50 °C for 2 days. The salts did not fully dissolve in DMF. The crude NG was precipitated in water, filtered, rinsed with water and transferred to a new filter paper to dry.

4.7.3 GMA-EGDMA-N$_3$ NG formation. GMA-EGDMA NG (96.7 mg, 0.3 mmol epoxides), sodium azide (9.4 mg, 0.15 mmol, 0.5 equiv.), ammonium chloride (48.8 mg, 0.9 mmol, 3 equiv.), and DMF (10 mL) were combined in a 25 mL round bottom flask, equipped with a magnetic stir bar and heated at 50 °C overnight. The salts did not fully dissolve in DMF. The crude NG was precipitated in water, filtered, rinsed with water and transferred to a new filter paper to dry resulting in a white solid (229 mg, ~43% conversion).

4.7.4 GMA-EGDMA-click formation. A click procedure was used as described in literature.[80] GMA-EGDMA-N$_3$ (10.15 mg, 15.4 μmol) was dissolved in DMF (0.5 mL) and stirred for 24 h to achieve maximum solubility. To a snap cap vial containing DCM (1.17 mL) was added 4-methyl-7-(prop-2-yn-1-yloxy)-2H-chromen-2-one (3.28 mg, 15.3 μmol). TBTA (1.53 mg, 2.9 μmol) and Cu(CH$_3$CN)$_4$PF$_6$ (0.89 mg, 2.4 μmol) were dissolved in MeOH (1.17 mL) resulting in a light blue solution. A N$_2$ purged RB flask fitted with a N$_2$ filled balloon, was charged with the NG solution, extra DMF (0.5 mL), the dye solution and the catalysts solution by means of N$_2$ flushed syringes. The light green, turbid reaction mixture turned pale yellow during the 24 h reaction and remained turbid. Solvents were removed under reduced pressure resulting in a yellow/green solid. The product was redissolved in DMF, the solids were filtered out and the solution was subjected to flash column chromatography (SiO$_2$, DMF).

4.7.5 GMA-EGDMA-NR$_3^+$ NG formation. GMA-EGDMA NG (105.5 mg, 0.3 mmol epoxides), N,N-dimethylethanolamine (62 μL, 0.6 mmol, 2 equiv.), DMF (9 mL) and H$_2$O (1 mL) were added to a 25 mL round bottom flask equipped with a magnetic stir bar and allowed to stir at 50 °C for 2 days. The reaction mixture was precipitated in diethyl ether, dissolved in H$_2$O, dialyzed for 4 days against water, MWCO = 1 kDa and freeze-dried resulting in a white solid (40 mg, 100% conversion).

4.7.6 GMA-EGDMA-OH NG formation. GMA-EGDMA NG (97.2 mg, 0.3 mmol epoxides), TFA (0.23 mL, 3 mmol, 10 equiv.), THF (9 mL) and H$_2$O (1 mL) were added to a 50 mL Erlenmeyer flask, equipped with a magnetic stir bar and allowed to stir overnight at room temperature. The solvents were removed in vacuo and the NG was redissolved in MeOH and precipitated in H$_2$O. The NG was dissolved in H$_2$O and dialyzed against water for 2 days, MWCO = 1 kDa. Freeze drying resulted in a white solid (100 mg, 100% conversion).

4.4.7 GMA-EGDMA-THG NG formation. GMA-EGDMA NG (96.8 mg, 0.3 mmol epoxides) and 1-thioglycerol (0.06 mL, 0.7 mmol, 2.5 equiv.) were dissolved in 9 mL DMF. LiOH

(6.9 mg, 0.3 mmol, 1 equiv.) was dissolved in 1 mL H_2O and added dropwise to the organic solution. The cloudy reaction mixture stirred at room temperature overnight. The NG was dispersed in H_2O and dialyzed against water for 3 days, MWCO = 1 kDa. Freeze drying resulted in a white solid (130 mg, 100% conversion).

4.4.8 GMA-EGDMA-boc NG formation. GMA-EGDMA NG (94.7 mg, 0.3 mmol epoxides) and 2-(Boc-amino)ethanethiol (0.12 mL, 0.7 mmol, 2.5 equiv.) were dissolved in 9 mL DMF. LiOH (24.7 mg, 1.0 mmol, 3.6 equiv.) was dissolved in 1 mL H_2O and added dropwise to the organic solution. The reaction mixture stirred overnight at room temperature becoming yellow and cloudy. The NG was dispersed in H_2O and dialyzed against water for 6 days, MWCO = 1 kDa. Water was removed under reduced pressure. The NG was dissolved in DCM, dried over $MgSO_4$, filtered, concentrated *in vacuo* and precipitated in hexane twice.

4.4.9 GMA-EGDMA-NH_3^+ NG formation. To a 12 mL colorless solution of **GMA-EGDMA-Boc** NG (0.29 mmol) in DCM was added TFA (0.11 mL, 1.4 mmol, 5 equiv.) and a magnetic stir bar. Upon addition of TFA the solution became yellow. The reaction was allowed to stir overnight forming sedimentation of NG that is no longer soluble in the organic solvents. Water was added to the reaction mixture and TFA and DCM were removed under reduced pressure. The aqueous solution was dialyzed against water for 2 days. Freeze drying yielded a white solid (90 mg, 100% conversion).

Author contributions

Anzar Khan and Jos M. J. Paulusse designed the study. Jeroen J. L. M. Cornelissen and Jos M. J. Paulusse guided the study. Disraëli N. M. Kusmus and Thijs van Veldhuisen conducted the experiments. Disraëli N. M. Kusmus drafted the manuscript. All authors approved the publication.

Conflicts of interest

There are no conflicts to declare.

Acknowledgements

Notes and references

1 M. Elsabahy, G. S. Heo, S.-M. Lim, G. Sun and K. L. Wooley, Polymeric nanostructures for imaging and therapy, *Chem. Rev.*, 2015, **115**(19), 10967–11011.

2 K. Riehemann, S. W. Schneider, T. A. Luger, B. Godin, M. Ferrari and H. Fuchs, Nanomedicine—challenge and perspectives, *Angew. Chem., Int. Ed.*, 2009, **48**(5), 872–897.

3 S. S. Kelkar and T. M. Reineke, Theranostics: combining imaging and therapy, *Bioconjug. Chem.*, 2011, **22**(10), 1879–1903.

4 N. T. Thanh and L. A. Green, Functionalisation of nanoparticles for biomedical applications, *Nano Today*, 2010, **5**(3), 213–230.

5 M. Elsabahy and K. L. Wooley, Design of polymeric nanoparticles for biomedical delivery applications, *Chem. Soc. Rev.*, 2012, **41**(7), 2545–2561.

6 A. Sharma, T. Garg, A. Aman, K. Panchal, R. Sharma, S. Kumar and T. Markandeywar, Nanogel—an advanced drug delivery tool: Current and future, *Artif. Cells Nanomed. Biotechnol.*, 2016, **44**(1), 165–177.

7 D. Steinhilber, T. Rossow, S. Wedepohl, F. Paulus, S. Seiffert and R. Haag, A microgel construction kit for bioorthogonal encapsulation and pH-controlled release of living cells, *Angew. Chem., Int. Ed.*, 2013, **52**(51), 13538–13543.

8 Y. Li, D. Maciel, J. Rodrigues, X. Shi and H. Tomas, Biodegradable polymer nanogels for drug/nucleic acid delivery, *Chem. Rev.*, 2015, **115**(16), 8564–8608.

9 A. V. Kabanov and S. V. Vinogradov, Nanogels as pharmaceutical carriers: finite networks of infinite capabilities, *Angew. Chem. Int. Ed.*, 2009, **48**(30), 5418–5429.

10 M. Molina, M. Asadian-Birjand, J. Balach, J. Bergueiro, E. Miceli and M. Calderón, Stimuli-responsive nanogel composites and their application in nanomedicine, *Chem. Soc. Rev.*, 2015, **44**(17), 6161–6186.

11 M. Fujioka-Kobayashi, M. S. Ota, A. Shimoda, K.-i. Nakahama, K. Akiyoshi, Y. Miyamoto and S. Iseki, Cholesteryl group-and acryloyl group-bearing pullulan nanogel to deliver BMP2 and FGF18 for bone tissue engineering, *Biomaterials*, 2012, **33**(30), 7613–7620.

12 Y. Xia, X. He, M. Cao, C. Chen, H. Xu, F. Pan and J. R. Lu, Thermoresponsive microgel films for harvesting cells and cell sheets, *Biomacromolecules*, 2013, **14**(10), 3615–3625.

13 M. M. Yallapu, M. Jaggi and S. C. Chauhan, Design and engineering of nanogels for cancer treatment, *Drug discovery today*, 2011, **16**(9–10), 457–463.

14 D. Dorwal, Nanogels as novel and versatile pharmaceuticals, *Int. J. Pharm. Pharm. Sci.*, 2012, **4**(3), 67–74.

15 S. Maya, B. Sarmento, A. Nair, N. S. Rejinold, S. V. Nair and R. Jayakumar, Smart stimuli sensitive nanogels in cancer drug delivery and imaging: a review, *Curr. Pharm. Des.*, 2013, **19**(41), 7203–7218.

16 G. Soni and K. S. Yadav, Nanogels as potential nanomedicine carrier for treatment of cancer: A mini review of the state of the art, *Saudi Pharm J*, 2016, **24**(2), 133–139.

17 U. Hasegawa, M. N. Shin-ichiro, S. C. Kaul, T. Hirano and K. Akiyoshi, Nanogel-quantum dot hybrid nanoparticles for live cell imaging, *Biochem. Biophys. Res. Commun.*, 2005, **331**(4), 917–921.

18 W. Wu, J. Shen, P. Banerjee and S. Zhou, Core–shell hybrid nanogels for integration of optical temperature-sensing, targeted tumor cell imaging, and combined chemo-photothermal treatment, *Biomaterials*, 2010, **31**(29), 7555–7566.

19 C. Zhao, Q. Chen, K. Patel, L. Li, X. Li, Q. Wang, G. Zhang and J. Zheng, Synthesis and characterization of pH-sensitive poly (N-2-hydroxyethyl acrylamide)–acrylic acid (poly (HEAA/AA)) nanogels with antifouling protection for controlled release, *Soft Matter*, 2012, **8**(30), 7848–7857.

20 A. W. Bridges, N. Singh, K. L. Burns, J. E. Babensee, L. A. Lyon and A. J. García, Reduced acute inflammatory responses to microgel conformal coatings, *Biomaterials*, 2008, **29**(35), 4605–4615.

21 H.-J. Kim, K. Zhang, L. Moore and D. Ho, Diamond nanogel-embedded contact lenses mediate lysozyme-dependent therapeutic release, *ACS Nano*, 2014, **8**(3), 2998–3005.

22 W. Wu, J. Shen, Y. Li, H. Zhu, P. Banerjee and S. Zhou, Specific glucose-to-SPR signal transduction at physiological pH by molecularly imprinted responsive hybrid microgels, *Biomaterials*, 2012, **33**(29), 7115–7125.

23 W. Wu, N. Mitra, E. C. Yan and S. Zhou, Multifunctional hybrid nanogel for integration of optical glucose sensing and self-regulated insulin release at physiological pH, *Acs Nano*, 2010, **4**(8), 4831–4839.

24 C. Li and S. Liu, Responsive nanogel-based dual fluorescent sensors for temperature and Hg2+ ions with enhanced detection sensitivity, *J. Mater. Chem.*, 2010, **20**(47), 10716–10723.

25 H. Zhu, Y. Li, R. Qiu, L. Shi, W. Wu and S. Zhou, Responsive fluorescent Bi2O3@ PVA hybrid nanogels for temperature-sensing, dual-modal imaging, and drug delivery, *Biomaterials*, 2012, **33**(10), 3058–3069.

26 W. Wu, J. Shen, Z. Gai, K. Hong, P. Banerjee and S. Zhou, Multi-functional core-shell hybrid nanogels for pH-dependent magnetic manipulation, fluorescent pH-sensing, and drug delivery, *Biomaterials*, 2011, **32**(36), 9876–9887.

27 H. s. Peng, J. A. Stolwijk, L. N. Sun, J. Wegener and O. S. Wolfbeis, A nanogel for ratiometric fluorescent sensing of intracellular pH values, *Angew. Chem.*, 2010, **122**(25), 4342–4345.

28 W. Wu, M. Aiello, T. Zhou, A. Berliner, P. Banerjee and S. Zhou, In-situ immobilization of quantum dots in polysaccharide-based nanogels for integration of optical pH-sensing, tumor cell imaging, and drug delivery, *Biomaterials*, 2010, **31**(11), 3023–3031.

29 T. Hoare, S. Young, M. W. Lawlor and D. S. Kohane, Thermoresponsive nanogels for prolonged duration local anesthesia, *Acta Biomater.*, 2012, **8**(10), 3596–3605.

30 J. K. Oh, R. Drumright, D. J. Siegwart and K. Matyjaszewski, The development of microgels/nanogels for drug delivery applications, *Prog. Polym. Sci.*, 2008, **33**(4), 448–477.

31 S. Nayak and L. A. Lyon, Soft nanotechnology with soft nanoparticles, *Angew. Chem. Int. Ed.*, 2005, **44**(47), 7686–7708.

32 S. Schubert, J. T. Delaney Jr and U. S. Schubert, Nanoprecipitation and nanoformulation of polymers: from history to powerful possibilities beyond poly (lactic acid), *Soft Matter*, 2011, **7**(5), 1581–1588.

33 E. Lepeltier, C. Bourgaux and P. Couvreur, Nanoprecipitation and the "Ouzo effect": Application to drug delivery devices, *Adv. Drug Deliv. Rev.*, 2014, **71**, 86–97.

34 J. P. Rolland, B. W. Maynor, L. E. Euliss, A. E. Exner, G. M. Denison and J. M. DeSimone, Direct fabrication and harvesting of monodisperse, shape-specific nanobiomaterials, *J. Am. Chem. Soc.*, 2005, **127**(28), 10096–10100.

35 D. Venturoli and B. Rippe, Ficoll and dextran *vs.* globular proteins as probes for testing glomerular permselectivity: effects of molecular size, shape, charge, and deformability, *Am. J. Physiol. Renal Physiol.*, 2005, **288**(4), F605–F613.

36 K.-I. Ogawara, M. Yoshida, K. Furumoto, Y. Takakura, M. Hashida, K. Higaki and T. Kimura, Uptake by hepatocytes and biliary excretion of intravenously administered polystyrene microspheres in rats, *J. Drug Target.*, 1999, **7**(3), 213–221.

37 C. Grazon, J. Rieger, N. Sanson and B. Charleux, Study of poly (N, N-diethylacrylamide) nanogel formation by aqueous dispersion polymerization of N, N-diethylacrylamide in the presence of poly (ethylene oxide)-b-poly (N, N-dimethylacrylamide) amphiphilic macromolecular RAFT agents, *Soft Matter*, 2011, **7**(7), 3482–3490.

38 P. Ding, J. Huang, C. Wei, W. Liu, W. Zhou, J. Wang, M. Wang, X. Guo, M. A. Cohen Stuart and J. Wang, Efficient and Generic Preparation of Diverse Polyelectrolyte Nanogels by Electrostatic Assembly Directed Polymerization, *CCS Chem.*, 2020, **2**(6), 1016–1025.

39 J.-H. Ryu, R. T. Chacko, S. Jiwpanich, S. Bickerton, R. P. Babu and S. Thayumanavan, Self-cross-linked polymer nanogels: a versatile nanoscopic drug delivery platform, *J. Am. Chem. Soc.*, 2010, **132**(48), 17227–17235.

40 R.-Q. Li, W. Wu, H.-Q. Song, Y. Ren, M. Yang, J. Li and F.-J. Xu, Well-defined reducible cationic nanogels based on functionalized low-molecular-weight PGMA for effective pDNA and siRNA delivery, *Acta Biomater.*, 2016, **41**, 282–292.

41 J. K. Oh, C. Tang, H. Gao, N. V. Tsarevsky and K. Matyjaszewski, Inverse miniemulsion ATRP: a new method for synthesis and functionalization of well-defined water-soluble/cross-linked polymeric particles, *J. Am. Chem. Soc.*, 2006, **128**(16), 5578–5584.

42 M. Hellmund, H. Zhou, O. Samsonova, P. Welker, T. Kissel and R. Haag, Functionalized polyglycerol amine nanogels as nanocarriers for DNA, *Macromol. Biosci.*, 2014, **14**(9), 1215–1221.

43 S. D. Sütekin and O. Güven, Application of radiation for the synthesis of poly (n-vinyl pyrrolidone) nanogels with controlled sizes from aqueous solutions, *Appl Radiat Isot .*, 2019, **145**, 161–169.

44 A. E. van der Ende, E. J. Kravitz and E. Harth, Approach to formation of multifunctional polyester particles in controlled nanoscopic dimensions, *J. Am. Chem. Soc.*, 2008, **130**, 8706–8713.

45 Y. Gao, B. Newland, D. Zhou, K. Matyjaszewski and W. Wang, Controlled Polymerization of Multivinyl Monomers: Formation of Cyclized/Knotted Single-Chain

Polymer Architectures, *Angew. Chem., Int. Ed.*, 2017, **56**(2), 450–460.

46 C. Boyer, V. Bulmus, T. P. Davis, V. Ladmiral, J. Liu and S. Perrier, Bioapplications of RAFT polymerization, *Chem. Rev.*, 2009, **109**(11), 5402–5436.

47 L. A. Picos-Corrales, A. Licea-Claveríe and K. F. Arndt, Core–shell nanogels by RAFT crosslinking polymerization: Synthesis and characterization, *J. Polym. Sci. A Polym. Chem.*, 2012, **50**(20), 4277–4287.

48 J. Rosselgong, S. P. Armes, W. Barton and D. Price, Synthesis of highly branched methacrylic copolymers: observation of near-ideal behavior using RAFT polymerization, *Macromolecules*, 2009, **42**(16), 5919–5924.

49 L. Nuhn, M. Hirsch, B. Krieg, K. Koynov, K. Fischer, M. Schmidt, M. Helm and R. Zentel, Cationic nanohydrogel particles as potential siRNA carriers for cellular delivery, *Acs Nano*, 2012, **6**(3), 2198–2214.

50 L. Nuhn, S. Gietzen, K. Mohr, K. Fischer, K. Toh, K. Miyata, Y. Matsumoto, K. Kataoka, M. Schmidt and R. Zentel, Aggregation behavior of cationic nanohydrogel particles in human blood serum, *Biomacromolecules*, 2014, **15**(4), 1526–1533.

51 L. Nuhn, S. Tomcin, K. Miyata, V. Mailänder, K. Landfester, K. Kataoka and R. Zentel, Size-dependent knockdown potential of siRNA-loaded cationic nanohydrogel particles, *Biomacromolecules*, 2014, **15**(11), 4111–4121.

52 F. Alexis, E. Pridgen, L. K. Molnar and O. C. Farokhzad, Factors affecting the clearance and biodistribution of polymeric nanoparticles, *Mol. Pharm.*, 2008, **5**(4), 505–515.

53 Y. Li, M. Beija, S. Laurent, L. v. Elst, R. N. Muller, H. T. Duong, A. B. Lowe, T. P. Davis and C. Boyer, Macromolecular ligands for gadolinium MRI contrast agents, *Macromolecules*, 2012, **45**(10), 4196–4204.

54 L. Hernández-Adame, C. Angulo, I. García-Silva, G. Palestino and S. Rosales-Mendoza, An overview of nanogel-based vaccines, *Expert Rev. Vaccines*, 2019, **18**(9), 951–968.

55 H. C. Kolb, M. G. Finn and K. B. Sharpless, Click Chemistry: Diverse Chemical Function from a Few Good Reactions, *Angew. Chem., Int. Ed.*, 2001, **40**(11), 2004–2021.

56 P. Y. Bruice, *Organic Chemistry*, 7th edn, Pearson: London, 2014.

57 H. Gao and K. Matyjaszewski, Synthesis of functional polymers with controlled architecture by CRP of monomers in the presence of cross-linkers: From stars to gels, *Prog. Polym. Sci.*, 2009, **34**(4), 317–350.

58 H. V. P. Thelu, S. Atchimnaidu, D. Perumal, K. S. Harikrishnan, S. Vijayan and R. Varghese, Self-assembly of an aptamer-decorated, DNA–protein hybrid nanogel: a biocompatible nanocarrier for targeted cancer therapy, *ACS Appl. Bio Mater.*, 2019, **2**(12), 5227–5234.

59 L. Wu, J. Zhang and W. Watanabe, Physical and chemical stability of drug nanoparticles, *Adv. Drug Deliv. Rev.*, 2011, **63**(6), 456–469.

60 H. C. Kolb, M. Finn and K. B. Sharpless, Click chemistry: diverse chemical function from a few good reactions, *Angew. Chem., Int. Ed.*, 2001, **40**(11), 2004–2021.

61 J. Weaver, I. Bannister, K. Robinson, X. Bories-Azeau, S. Armes, M. Smallridge and P. McKenna, Stimulus-responsive water-soluble polymers based on 2-hydroxyethyl methacrylate, *Macromolecules*, 2004, **37**(7), 2395–2403.

62 E. M. Muzammil, A. Khan and M. C. Stuparu, Post-polymerization modification reactions of poly (glycidyl methacrylate) s, *RSC Adv.*, 2017, **7**(88), 55874–55884.

63 I. Gadwal, M. C. Stuparu and A. Khan, Homopolymer bifunctionalization through sequential thiol–epoxy and esterification reactions: an optimization, quantification, and structural elucidation study, *Polym. Chem.*, 2015, **6**(8), 1393–1404.

64 J. Hwang, Y. Choe, J. Bang and A. Khan, Scalable ambient synthesis of water-soluble poly (β-hydroxythio-ether) s, *J. Polym. Sci. A Polym. Chem.*, 2017, **55**(20), 3381–3386.

65 J. Hwang, D. G. Lee, H. Yeo, J. Rao, Z. Zhu, J. Shin, K. Jeong, S. Kim, H. W. Jung and A. Khan, Proton Transfer Hydrogels: Versatility and Applications, *J. Am. Chem. Soc.*, 2018.

66 M. C. Stuparu and A. Khan, Thiol-epoxy "click" chemistry: Application in preparation and postpolymerization modification of polymers, *J. Polym. Sci. A Polym. Chem.*, 2016, **54**(19), 3057–3070.

67 X. Yang, M. Chai, Y. Zhu, W. Yang and F. Xu, Facilitation of gene transfection with well-defined degradable comb-shaped poly (glycidyl methacrylate) derivative vectors, *Bioconjug. Chem.*, 2012, **23**(3), 618–626.

68 R. Li, Y. Niu, N. Zhao, B. Yu, C. Mao and F. Xu, Series of new β-cyclodextrin-cored starlike carriers for gene delivery, *ACS Appl. Mater. Interfaces*, 2014, **6**(6), 3969–3978.

69 R. Li, Y. Hu, B. Yu, N. Zhao and F. Xu, Bioreducible comb-shaped conjugates composed of secondary amine and hydroxyl group-containing backbones and disulfide-linked side chains with tertiary amine groups for facilitating gene delivery, *Bioconjug. Chem.*, 2014, **25**(1), 155–164.

70 X.-C. Yang, Y.-L. Niu, N.-N. Zhao, C. Mao and F.-J. Xu, A biocleavable pullulan-based vector *via* ATRP for liver cell-targeting gene delivery, *Biomaterials*, 2014, **35**(12), 3873–3884.

71 X. Dou, M. Chai, Y. Zhu, W. Yang and F. Xu, Aminated poly (glycidyl methacrylate) s for constructing efficient gene carriers, *ACS Appl. Mater. Interfaces*, 2013, **5**(8), 3212–3218.

72 H. Gao, M. Elsabahy, E. V. Giger, D. Li, R. E. Prudhomme and J.-C. Leroux, Aminated linear and star-shape poly (glycerol methacrylate) s: synthesis and self-assembling properties, *Biomacromolecules*, 2010, **11**(4), 889–895.

73 M. Ma, F. Li, F. j. Chen, S. x. Cheng and R. x. Zhuo, Poly (ethylene glycol)-block-Poly (glycidyl methacrylate) with Oligoamine Side Chains as Efficient Gene Vectors, *Macromol. Biosci.*, 2010, **10**(2), 183–191.

74 S. Edmondson and W. T. Huck, Controlled growth and subsequent chemical modification of poly (glycidyl methacrylate) brushes on silicon wafers, *J. Mater. Chem.*, 2004, **14**(4), 730–734.

75 A. V. Kabanov and S. V. Vinogradov, Nanogels as pharmaceutical carriers: finite networks of infinite capabilities, *Angew. Chem., Int. Ed.*, 2009, **48**(30), 5418–5429.

76 N. V. Tsarevsky, S. A. Bencherif and K. Matyjaszewski, Graft copolymers by a combination of ATRP and two different consecutive click reactions, *Macromolecules*, 2007, **40**(13), 4439–4445.

77 M. Chini, P. Crotti and F. Macchia, Efficient metal salt catalyzed azidolysis of epoxides with sodium azide in acetonitrile, *Tetrahedron Lett.*, 1990, **31**(39), 5641–5644.

78 E. Mauri, I. Moroni, L. Magagnin, M. Masi, A. Sacchetti and F. Rossi, Comparison between two different click strategies to synthesize fluorescent nanogels for therapeutic applications, *React. Funct. Polym.*, 2016, **105**, 35–44.

79 C. J. Ferguson, R. J. Hughes, D. Nguyen, B. T. Pham, R. G. Gilbert, A. K. Serelis, C. H. Such and B. S. Hawkett, Ab initio emulsion polymerization by RAFT-controlled self-assembly, *Macromolecules*, 2005, **38**(6), 2191–2204.

80 C. Nicosia, S. O. Krabbenborg, D. N. Reinhoudt and J. Huskens, In situ fluorimetric detection of micrometer-scale pH gradients at the solid/liquid interface, *Supramol. Chem.*, 2013, **25**(9–11), 756–766.

81 S. Bräse, C. Gil, K. Knepper and V. Zimmermann, Organic azides: an exploding diversity of a unique class of compounds, *Angew. Chem., Int. Ed.*, 2005, **44**(33), 5188–5240.